Study of PET/PP/TiO_2 Microfibrillar-Structured Composites, Part 1: Preparation, Morphology, and Dynamic Mechanical Analysis of Fibrillized Blends

Wenjing Li,[1] Alois K. Schlarb,[1] Michael Evstatiev[2]

[1]*Institut für Verbundwerkstoffe, (Institute for Composite Materials) University of Kaiserslautern, Erwin Schrödinger Str., 67663 Kaiserslautern, Germany*
[2]*Laboratory on Polymers, Sofia University, 1126 Sofia, Bulgaria*

Received 22 September 2008; accepted 2 January 2009
DOI 10.1002/app.29993
Published online 14 April 2009 in Wiley InterScience (www.interscience.wiley.com).

ABSTRACT: The objective of this study was to manufacture and investigate a novel microfibrillar-reinforced material based on fibrillized blends of polyethyleneterephthalate (PET), polypropylene (PP), and TiO_2 nanoparticles (300 nm and 15 nm in size). The uncompatibilized and compatibilized blends (polypropylene grafted maleic anhydride as compatibilizer) were extruded and subsequently cold-drawn into strands with a draw ratio of 10. The effects of compatibilizer and TiO_2 particles on the structure and properties of drawn strands were investigated. Upon addition of compatibilizer, the preferential location of TiO_2 particles shifted from the PET-dispersed phase to the PP matrix, which brought about different structures of the drawn strands. Differential scanning calorimetry study provided indications for a heterogeneous nucleation effect of the PET fibrils on the PP matrix and of the TiO_2 particles on the PET fibrils. Dynamic mechanical analysis demonstrated that the mechanical properties of the drawn strands are strongly dependent on the strand structures.
 J Appl Polym Sci 113: 1471–1479, 2009

Key words: blends; nanoparticles; microfibrils; dispersions; interfaces

INTRODUCTION

To get synergistically combined properties of two or more polymers, the polymer blends are widely investigated. As common knowledge, a great number of the polymers are immiscible, therefore a phase separation, i.e., a matrix and a dispersed phase, can occur during processing of immiscible polymer blends.[1] Due to different rheological properties, the components, and different processing conditions, the dispersed phase might have distinct morphologies (spheres, ellipsoids, fibrils, and plates) among which a fibril shape of the dispersed phase seems to be favorable for mechanical properties of the composites. To generate in situ formed fibrils in polymer blends, the so-called microfibrillar reinforced composites (MFC) concept was proposed.[2–4] Unlike the classical macrocomposites (e.g., fiber-reinforced macrocomposites), this group of polymer composites is reinforced with polymer fibrils or, more frequently, bundles of them.[2–5,6] The preparation of MFC includes three technical steps: (1) the mixing step, melt blending of two immiscible polymers having different melting temperatures; (2) the fibrillization step, cold drawing of the blend to get orientation of the two phases; (3) the isotropization step, thermal treatment at a temperature between the melting temperatures of the two components.[5,6–10] Several immiscible polymer pairs for manufacturing MFC have been studied,[6–9] among which the polyethleneterephthalate/polypropylene (PET/PP) combination receives special attention since the dispersed phase and the matrix impart, respectively, high stiffness and toughness to the composite.[10–12]

Addition of inorganic nanofillers into single-phase polymer was shown to change its mechanical properties.[13,14] For formulating high-performance polymer blends, nanofillers have been introduced into binary polymer blends in recent years. It was reported that incorporation of nanoparticles and nanoclays into polymer blends can effectively reduce the domain size and increase the compatibility of the two phases.[15–17] Li introduced carbon black into the PET/PE system, and the CB/PET/PP MFC were prepared. The carbon black is found exclusively located in the PET microfibrils and leads to a sharp drop in volume resistivity.[18,19] To our knowledge, besides this report there is no other investigation concerning the nanoparticle-filled MFC. It is of particular interest to investigate the effect of nanofillers on the morphology and properties of MFC. In the

Correspondence to: W. Li (wenjing.li@ivw.uni-kl.de).
Contract grant sponsors: BASF Chemical Company.

TABLE I
Material Designation and Composition

Designation	Composition	Parts (volume ratio)
PET/PP	PET/PP	25/75
PET/PP/C	PET/PP/PP-*g*-MA	25/72/3
PET/PP/2T300	PET/PP/TiO_2-300 nm	24.5/73.5/2
PET/PP/C/2T300	PET/PP/PP-*g*-MA/TiO_2-300 nm	24.5/70.5/3/2
PET/PP/4T300	PET/PP/TiO_2-300 nm	24/72/4
PET/PP/C/4T300	PET/PP/PP-*g*-MA/TiO_2-300 nm	24/69/3/4
PET/PP/2T15	PET/PP/TiO_2-15 nm	24.5/73.5/2
PET/PP/C/2T15	PET/PP/PP-*g*-MA/TiO_2-15 nm	24.5/70.5/3/2

present work, TiO_2 nanoparticles were incorporated into the PET/PP blend, both PET/PP and PET/PP/TiO_2 drawn strands were prepared, some of the drawn strands also comprise 3 vol % of PP-*g*-MA as a compatibilizing agent. The structures of drawn strands were characterized by scanning electron microscope (SEM) and differential scanning calorimetry (DSC). The effects of the TiO_2 nanoparticles and their dimensions on the structure and mechanical properties of the fibrillized blends were studied.

EXPERIMENTAL

Materials

PET (skyPET BL8050) was provided by SK Chemicals (Warszawa, Poland) with the intrinsic viscosity of 0.80 dL/g, and PP was purchased from Basell (Novolen). PP-*g*-MA supplied by ATOfina (OREVAC CA 100, Colombes Cedex, France) was used as the compatibilizer for PET and PP. Two types of TiO_2 nanoparticles (Kronos 2220 and RM300) were supplied by Kronos (Leverkusen, Germany) and Sachtleben Chemie GmbH (Duisburg, Germany), respectively. The mean diameters of the two nanoparticles were 300 nm for Kronos 2220 and 15 nm for RM300, respectively. Both types were used as received.

Sample preparation

Neat PET was dried for 12 h at 100°C to avoid the hydrolytic degradation during extrusion. PP-*g*-MA was dried for 12 h at 80°C. PP was first extruded with 4 or 7 vol % of the TiO_2 (both Kronos 2220 and RM300) in a Berstorff twin-screw extruder using an optimized extrusion technique.

The obtained PP/TiO_2 nanocomposite was then premixed with PET in presence (or absence) of PP-*g*-MA. The premixed materials were melted and extruded in a Brabender twin-screw extruder (Brabender® GmbH and Co. KG, Duisburg, Germany) under the screw speed of 40 rpm. The temperature zones from hopper to die were set at 230, 270, 275, and 275°C. For comparison purposes, PET/PP blends with and without PP-*g*-MA were also extruded in the Brabender extruder under the same condition. The designation and composition of the nanocomposites and polymer blends are given in Table I.

After removal from the extruder (2-mm capillary die), the extrudate was immediately cooled down to 85°C and drawn by a stretching device, as described before.[6,20,21] The draw ratio defined as the ratio between the cross-sectional areas of the drawn strand, and the die was kept at 10.

Characterization

The cryo-fractured surfaces of extrudates were inspected using SEM (JEOL JSM-6300 of JEOL Ltd., Tokyo, Japan and ZEISS Supra™ 40VP of Carl Zeiss GmbH, Goettingen). For the drawn strands, the PP phase was selectively etched by hot xylene at 130°C for 4 h.

DSC traces of drawn strands were obtained by using a Mettler Toledo (Giessen, Germany), DSC821 device. In the first heating run, the specimen was heated from room temperature to 200°C and then cooled down to 40°C; in the second heating run, the specimen was reheated to 280°C and kept at this temperature for 3 min and finally cooled down to 40°C. The heating and cooling rates were kept at 20°C/min. The percent of crystallinity was calculated by using $\Delta H_f^0 = 209$ J/g for PP[22] and $\Delta H_f^0 = 140$ J/g for PET.[12]

Dynamic mechanical analysis (DMA) of drawn strands was carried out using a DMA Q800 apparatus (TA Instrument, New Castle, Delaware) from −50 to 150°C. The storage modulus (E') and mechanical damping factor (tan δ) of the drawn strands were measured. All measurements were conducted in tensile and strain control modes at a fixed frequency of 1 Hz with a heating rate of 3°C/min. The strain was kept at 0.1%.

RESULTS AND DISCUSSION

Dispersion of TiO_2 particles in PET/PP blends

Figure 1 shows the fracture surfaces of the PET/PP/TiO_2 extrudates. For comparison purposes, the SEM images of PP/PET and PET/PP/C blends are also

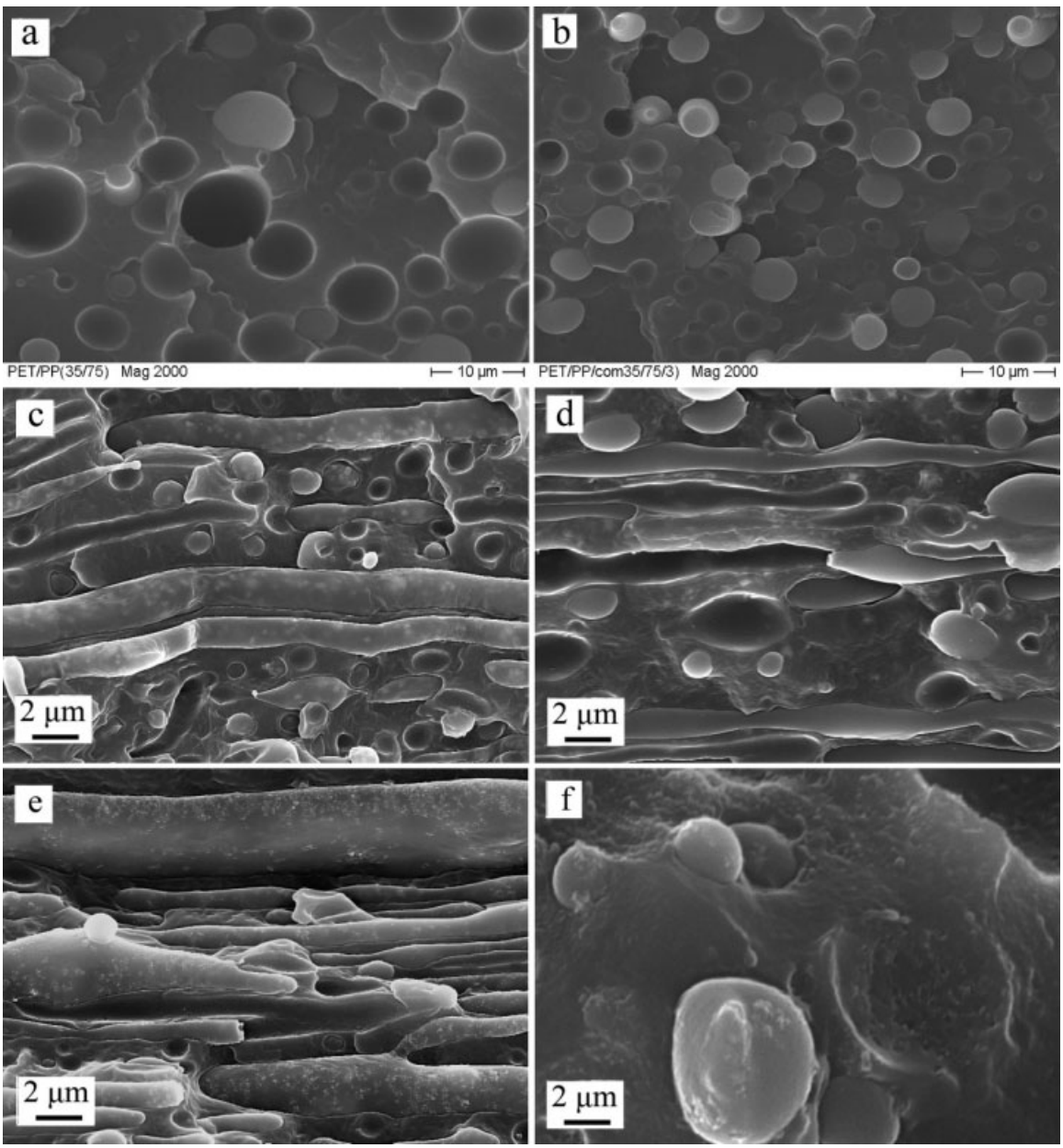

Figure 1 SEM images of PET/PP and PET/PP/TiO_2 extrudates: (a) PET/PP, (b) PET/PP/C, (c) PET/PP/2T300, (d) PET/PP/C/2T300, (e) PET/PP/2T15, (f) PET/PP/C/2T15.

presented. In the PET/PP/2T300 extrudate, the TiO_2-300 nm particles disperse uniquely in the cylindrical PET phase [Fig. 1(c)]. Interestingly, as can be seen from Figure 1(d), in the compatibilized extrudate, PET/PP/C/2T300, the TiO_2-300 nm particles are only found in the PP matrix. When the TiO_2-15 nm nanoparticles are incorporated into the blend, for the extrudate without compatibilizer, all the nanoparticles migrate into PET phase [Fig. 1(e)]; with compatibilizer, however, the nanoparticles are found in the PET-dispersed phase, in the PP matrix, as well as at the interface [Fig. 1(f)].

Compared with the nonpolar PP, the TiO_2 particles are more prone to interacting with the polar PET, since the $\gamma_{TiO2\text{-}PET}$ (interfacial tension between TiO_2 and PET) is lower than $\gamma_{TiO2\text{-}PP}$. Therefore in the PET/PP/2T300 and PET/PP/2T15 nanocomposites, the TiO_2 particles are exclusively located in the PET phase. MA (maleic anhydride) is known to be an excellent ligand for metal oxides; it can be easily adsorbed onto the TiO_2 surface by electronic donation.[23] Upon addition of PP-*g*-MA, the surface of TiO_2 particles is coated with the PP chains, which make the TiO_2 compatible with the PP. Therefore in the PET/PP/C/2T300, the TiO_2-300 nm particles are located in the PP phase. Compared with the TiO_2-300 nm particles, the specific surface area of the TiO_2-15 nm nanoparticles is much higher. At the

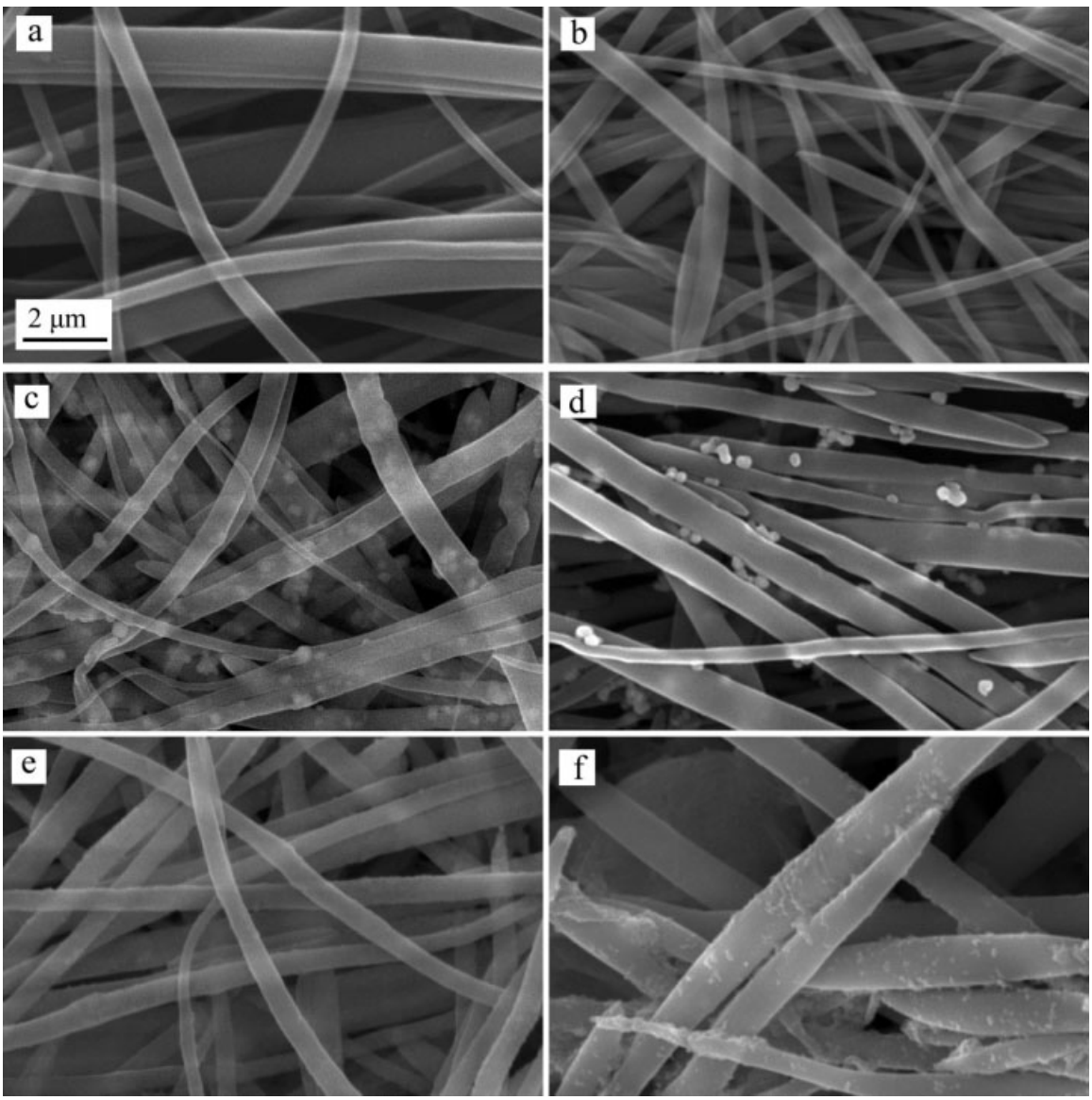

Figure 2 SEM images of the PET fibrils in drawn strands, PP was removed by hot xylene: (a) PET/PP, (b) PET/PP/C, (c) PET/PP/2T300, (d) PET/PP/C/2T300, (e) PET/PP/2T15, (f) PET/PP/C/2T15.

same concentration of PP-*g*-MA (3 vol %), some TiO_2-15 nm nanoparticles remain uncoated. They are still driven into the thermodynamically favored PET phase.

Morphology of PET fibrils

As is well known, during cold drawing of the extrudates of the immiscible polymer blends, both phases transform into fibrils.[2–6,20,21,24,25] To get better information about the size and aspect ratio of the PET fibrils in the drawn strands, the PP phase was removed by hot xylene. Figure 2(a) shows the microphotograph of the PET fibrils with the diameters in a range of 0.5–1.5 μm and a high aspect ratio. However, for the PET/PP/C drawn strand, some short needle-like PET formations are seen beside the long fibrils [Fig. 2(b)]. Figure 2(c,d) shows the PET fibrils in the PET/PP/2T300 and PET/PP/C/2T300 drawn strands, respectively. The observation confirms that the TiO_2-300 nm particles have a preferential location in one polymer phase, as seen in the extrudates (Fig. 1). In the PET/PP/2T300 drawn strand, it is clearly seen that the TiO_2-300 nm particles are in the PET phase. While in the PET/PP/C/2T300 one, the particles are preferentially located in PP and partially washed away by hot xylene. Therefore only those located at the PET/PP interface are seen. In like manner, for the etched PET/PP/C/2T15 drawn strand, the PET fibrils are covered with the small agglomerates of the TiO_2-15 nm nanoparticles [Fig. 2(f)], whereas in the etched PET/PP/2T15 one, no agglomerates are found on the fibril surface [Fig. 2(e)].

TABLE II
Crystallization Temperature (T_c) and Crystallinity (X_{cr}) of PP and PET in Drawn Strands

Sample	First cooling run		Second cooling run	
	T_c of PP (°C)	X_{cr} of PP (%)	T_c of PET (°C)	X_{cr} of PET (%)
Neat PP	111.0	49.6	–	–
PP/TiO_2(300 nm)-2 vol %	119.6	45.0	–	–
PET/PP	121.0	49.8	181.2	13.1
PET/PP/C	121.5	50.4	–	–
PET/PP/2T300	121.5	45.2	184.0	16.0
PET/PP/C/2T300	121.6	42.9	–	–
PET/PP/4T300	121.7	40.9	186.3	21.4
PET/PP/C/4T300	122.4	42.8	–	–
PET/PP/2T15	122.1	44.3	185.5	18.3
PET/PP/C/2T15	122.3	44.4	–	–

It should be pointed out that similar to the compatibilized PET/PP drawn strands, numbers of needle-like PET formations are also noticed in the compatibilized PET/PP/TiO_2 drawn strands [Fig. 2(d,f)]. During stretching of the extrudates, the dispersed PET droplets are elongated. Depending on their original size, the PET droplets are either deformed into fibrils with large aspect ratio or needle-like formations. In the PET/PP/C blend, due to the compatibilization effect of PP-*g*-MA, a smaller PET droplet size in the extrudate is expected. Therefore in the drawn strand, the needle-like PET formations are seen. For the PET/PP/C/2T300 and PET/PP/C/2T15 nanocomposites, the preferential location of TiO_2 particles in the PP phase increases the viscosity of PP. The more viscous matrix facilitates the droplets breakup. These small PET droplets are deformed into needle-like formations after stretching the extrudate.

DSC results

The crystallization temperatures (T_c) and degree of crystallinities (X_{cr}) of the PP and PET in drawn strands are presented in Table II. For comparison, neat PP and PP/TiO_2(300 nm)-2 vol % drawn strands were also subjected to DSC characterization. During the first cooling run (the PET fibrils are kept), the crystallization temperature of the PP in the PET/PP and PET/PP/TiO_2 drawn strands is about 10°C higher than that of the neat PP. The heterogeneous nucleation effect of the PET fibrils on the PP matrix is believed to be responsible for this elevation of T_c. The preferential location of TiO_2 particles does not help to further increase the T_c of the PP.

Incorporation of the TiO_2 particles into PET/PP moderately decreases the crystallinity of the PP irrespective of their preferential locations (in the PP phase or on the PET phase). To the same degree, the decrease in crystallinity of PP is also observed in the PP/TiO_2(300 nm)-2 vol % drawn strand. Numerous researchers have reported similar observations: the crystallinity of polymer matrix is decreased upon addition of nanofillers.[26–28] In the compatibilized PET/PP/TiO_2 drawn strands, the TiO_2 particles are preferentially located in the PP matrix. The presence of the high concentrations of TiO_2 particles prevents large crystalline domains from forming due to the restrictions imposed on polymer chains. This leads to smaller crystallite structures and more defects in the crystalline lamella. Accordingly, the crystallinity of PP is decreased.[28,29] In the uncompatibilized PET/PP/TiO_2 drawn strands, the TiO_2 particles are preferentially located in the PET. However, we cannot explain the decreased crystallinity of PP.

In the second cooling run, the crystallization peak of the PET disappears upon addition of compatibilizer. A similar result was also found by Bae for PET/PP-*g*-HI blend.[30] It was suggested that the in situ generated PP-*g*-PET copolymer that locates in the PET phase may act as a polymeric diluent to retard the crystallization of the PET and level off the heat of crystallization of the PET. However, for the uncompatibilized PET/PP/TiO_2 drawn strands where the TiO_2 particles are in the PET phase, the T_c and crystallinity of the PET is elevated. It is supposed that the TiO_2 particles serve as nucleation sites for the PET and elevate the crystallization temperature.

Dynamic mechanical analysis

Generally, incorporation of nanofillers into single-phase polymer or polymer blend was reported to increase the modulus of the composites.[31,32] In our study, neat PP and PP/TiO_2(300 nm)-2 vol % drawn strands with the same draw ratio (draw ratio 10) were prepared, and the DMA results are presented in Figure 3. The storage modulus (E') of the PP drawn strand shows a dramatic increase compared with bulk PP (generally the modulus of bulk PP at room temperature is less than 1800 MPa), which is attributed to the orientation of molecular chain after

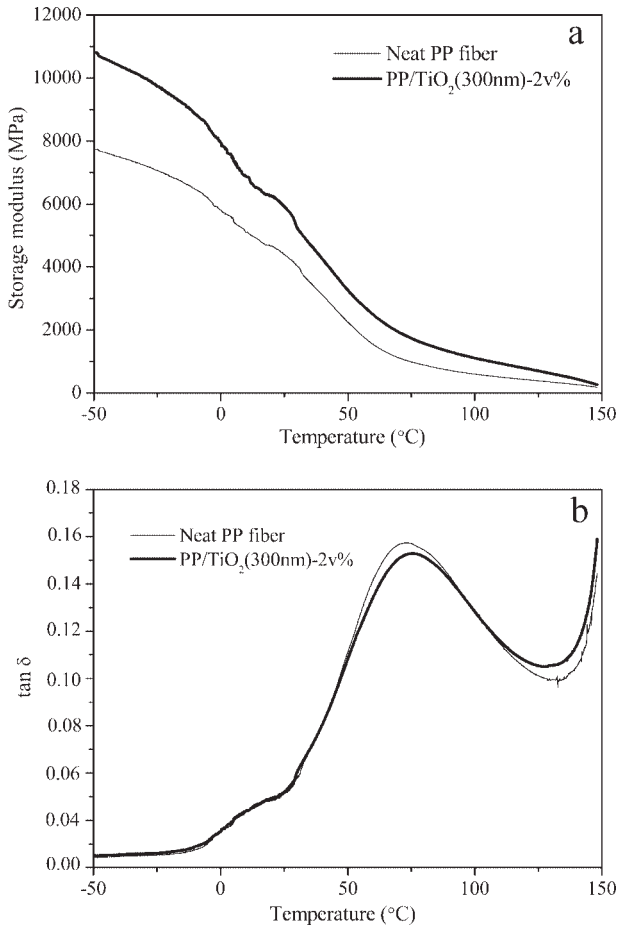

Figure 3 DMA spectra of neat PP and PP/TiO_2 drawn strands: (a) storage modulus vs. temperature, (b) tan δ vs. temperature.

stretching. Incorporation of the TiO_2-300 nm particles further increases the E' of the PP drawn strand in the whole temperature range. It can be seen from Figure 3(b) that with TiO_2-300 nm particles the T_g of PP shifts to a higher temperature. The elevation of T_g can be related to the reduction in mobility of the PP macromolecular chains in the vicinity of the fillers, which indicates a good filler–matrix interaction.[33]

In case of the PET/PP/TiO_2 drawn strands, both the PET and PP phases are oriented; therefore the interface between the two phases becomes critical for the mechanical properties. The DMA result of the drawn strands is presented in Figure 4(a) in terms of temperature dependence of the storage modulus. The PET/PP drawn strand shows the highest modulus because of the reinforcement effect of PET fibrils and a comparatively good interfacial adhesion between the reinforcement and matrix. Incorporation of TiO_2 decreases the E' for all drawn strands, and the E' drops even more with increasing concentration of TiO_2. The decrease of E' by incorporating the TiO_2 particles is supposed to be mainly related to the decrease of matrix–fibril interfacial adhesion and to the formation of defects at the interface. As a result, the stress transfer from matrix to fibrils during DMA tests becomes less effective and the E' drops accordingly.

Figure 5(a) presents the morphology of the PET/PP/2T300 drawn strand. After stretching, some TiO_2-300 nm particles protrude out of the PET fibril, thus leaving pits on the interface. Therefore, the interface of the PET fibrils and the PP matrix is damaged, and interfacial defects appear. Some TiO_2 particles even lose their adhesion to the PET, which creates large voids in the PET fibrils (indicated by arrows). Figure 5(b) shows that in the PET/PP/C/2T300 extrudate, the thickness of the PP/TiO_2 phase between the neighboring elongated PET droplets is quite small (indicated by arrows), and in some parts it is less than 800 nm. In the drawn strand, this thickness decreases dramatically, forming a thin film that is not able to encapsulate the TiO_2-300 nm particles [Fig. 5(c)]. Therefore these TiO_2 particles generate defects at the interface and result in the drop of the E'. To better illustrate the formation of the PP

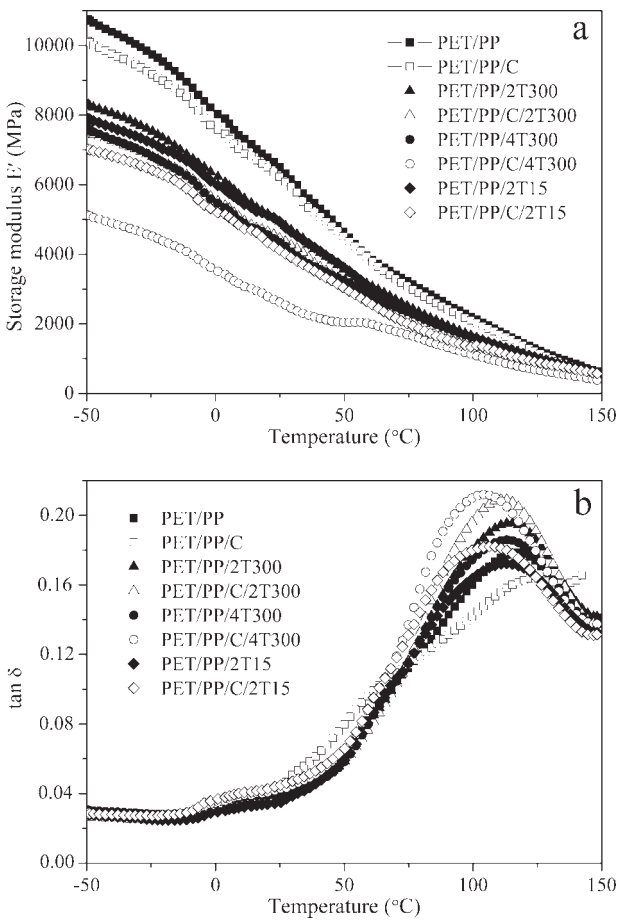

Figure 4 DMA spectra of PET/PP and PET/PP/TiO_2 drawn strands: (a) storage modulus vs. temperature, (b) tan δ vs. temperature.

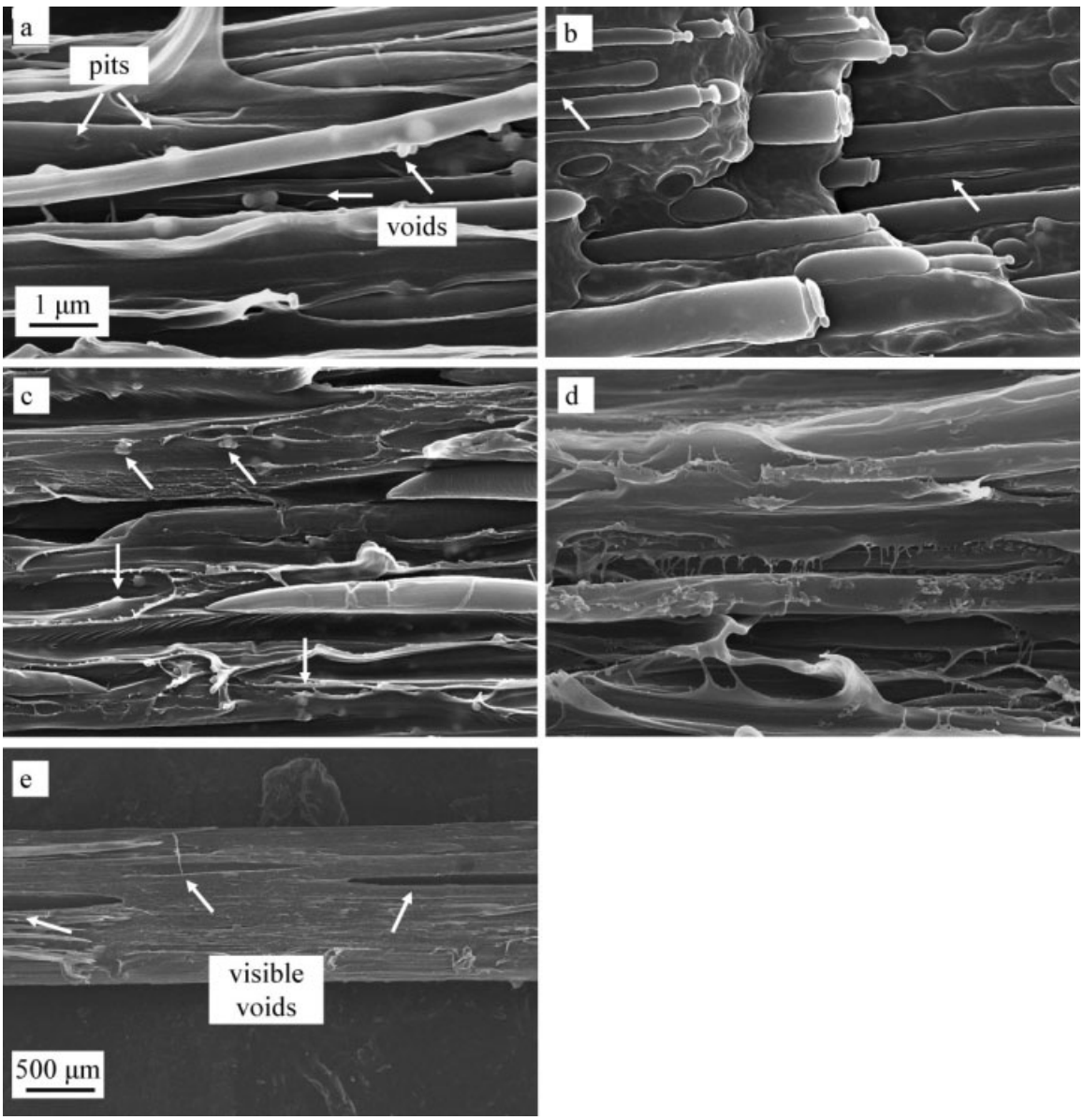

Figure 5 SEM images of the drawn strands and slightly drawn extrudates: (a) PET/PP/2T300 drawn strand, (b) PET/PP/C/2T300 slightly drawn extrudate, (c) PET/PP/C/2T300 drawn strand, (d) PET/PP/2T15 drawn strand, (e) PET/PP/2T15 drawn strand at low magnification.

thin film and the voids at the interface, a schematic graph is presented in Figure 6.

For the PET/PP/2T15 and PET/PP/C/2T15 drawn strands in which the TiO_2-15 nm nanoparticles are always found in the PET fibrils, the situation is more complicated. First, the PET fibrils are somehow damaged by the agglomerates of TiO_2-15 nm nanoparticles as shown in Figure 5(d). Second, visible voids appear in the drawn strands [see Fig. 5(e)]. Both structures cause the decrease of E' [Fig. 4(a)].

In general, the incorporated TiO_2 particles reduce the fibrillation ability of PET phase, resulting in poor fibril morphology, which further affects the property enhancement of the PET/PP/TiO_2 drawn strand.

It is interesting to notice that the uncompatibilized drawn strands always exhibit a higher modulus than the compatibilized ones, irrespective of the presence of the TiO_2 particles. In the compatibilized drawn strands, some PET fibrils are replaced by short needle-like PET formations; therefore the fibril reinforcement is less effective. Besides, the elastomeric nature of the compatibilizer (PP-*g*-MA) may also decrease the E' of the drawn strands.[34]

Figure 4(b) shows the tan δ vs. temperature curves for the drawn strands. The dominant peak that appears at around 100°C is correspondent to the glass transition temperature (T_g) of the PET.[35] The small shoulder that locates in the vicinity of 10°C is believed to be the β transition of the PP. According

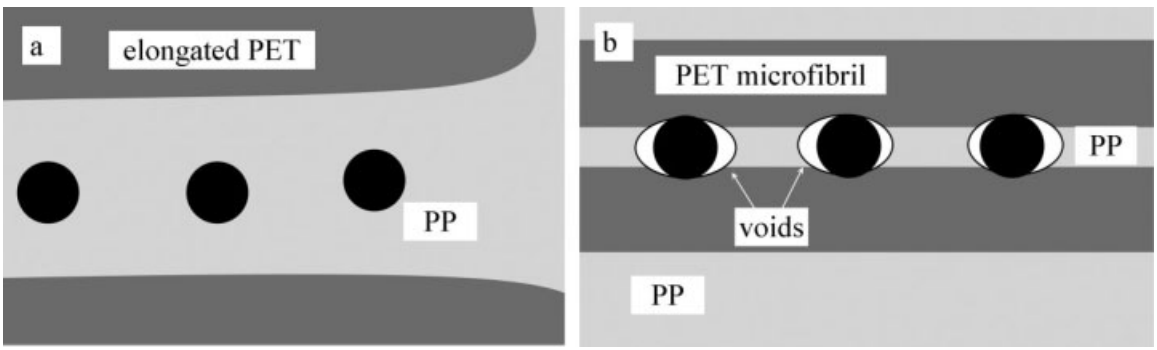

Figure 6 Schematic representation of (a) slightly drawn PET/PP/2T300 extrudate and (b) PET/PP/2T300 drawn strand.

to McCrum,[36] PP exhibits three relaxations that are γ (at -80°C), β (at 10°C), and α (at 100°C) transitions. The β transition is due to the relaxing unit consisting of a few chain segments in the amorphous regions, and the temperature of β maximum is taken as T_g.

The T_g of the PET component in the compatibilized PET/PP/TiO_2 drawn strands is noticeably lower than that of the PET in the uncompatibilized ones. On the one hand, for the compatibilized drawn strands, compatibility between the PET and the PP is improved upon addition of compatibilizer; therefore the T_g of PET shifts toward that of the PP. On the other hand, in the uncompatibilized PET/PP/TiO_2 drawn strands, the TiO_2 particles are located in the PET fibrils and the interaction between TiO_2 particles and the PET will result in the shifts of the T_g toward a higher temperature. Both the two factors account for the noticeable difference of the T_g for the PET phase in the compatibilized and uncompatibilized PET/PP/TiO_2 drawn strands.

The dominate damping peak of the PET/PP/TiO_2 drawn strands exhibits an increase magnitude compared with the PET/PP drawn strands, which also indicates the poor interfacial adhesion between the microfibrils and the matrix. In a composite system, damping is affected through the incorporation of fibers. The composite with poor interfacial bonding between fibers and matrix tends to dissipate more energy, thus resulting in an increase magnitude of damping peak.[37]

CONCLUSIONS

TiO_2 particles with two different sizes (300 nm and 15 nm) were incorporated into the PET/PP blend, and the PET/PP/TiO_2 drawn strands were obtained. Structures and properties of the drawn strands were found to be strongly influenced by incorporating TiO_2 particles and compatibilizer. The conclusions are listed as follows:

1. In the uncompatibilized PET/PP/TiO_2 extrudates, the TiO_2 particles migrate from the PP matrix to the PET dispersed phase during melt blending of PP/TiO_2 and PET; whereas in the compatibilized extrudates, the TiO_2 particles stay in the PP matrix.
2. The T_c of the PP in drawn strands is dramatically increased because of heterogeneous nucleation of the PET fibrils. The T_c of the PET in the uncompatibilized drawn strands is also elevated because the TiO_2 particles act as nucleation agent for PET.
3. Incorporation of the TiO_2 particles in the drawn strands results in a decrease of the storage modulus compared with the PET/PP drawn strand. In the presence of TiO_2 particles, defects appear at the interface between the PET fibrils and the PP matrix, which leads to poor stress transfer and thereby a drop of E'. The T_g of the PET in the compatibilized PET/PP/TiO_2 drawn strands is lower than in the uncompatibilized ones.

The authors thank Mr. Walter and Ms. Knör for the extrusion of materials and Dr. Ga Zhang for helpful discussions.

References

1. Paul, D. R.; Newman, S. Polymer Blends; Academic Press: New York, 1978.
2. Evstatiev, M.; Fakirov, S. Polymer 1992, 33, 877.
3. Fakirov, S.; Evstatiev, M.; Schultz, J. M. Polymer 1993, 34, 4669.
4. Fakirov, S.; Evstatiev, M.; Petrovich, S. Macromolecules 1993, 26, 5219.
5. Fakirov, S.; Evstatiev, M.; Friedrich, K. In Polymer Blends; Paul, D. R.; Bucknall, C. B., Eds.; Wiley: New York, 2000, Vol. 2, p 455.
6. Evstatiev, M.; Schultz, J. M.; Fakirov, S.; Friedrich, K. Polym Eng Sci 2001, 41, 192.
7. Li, Z. M.; Fu, X. R.; Yang, S. Y.; Yang, M. B.; Yang, W.; Huang, R. Polym Eng Sci 2004, 44, 1561.
8. Quan, H.; Zhong, G. J.; Li, Z. M.; Yang, M. B.; Xie, B. H. Polym Eng Sci 2005, 45, 1303.
9. Leung, K. L.; Easteal, A.; Bhattacharyya, D. Compos A 2008, 39, 662.
10. Li, Z. M.; Li, L. B.; Shen, K. Z.; Yang, M. B.; Huang, R. J Polym Sci Part B: Polym Phys 2004, 42, 4095.

11. Taepaiboon, P.; Junkasem, J.; Dangtungee, R.; Amornsakchai, T.; Supaphol, P. J Appl Polym Sci 2006, 102, 1173.
12. Fuchs, C.; Bhattacharyya, D.; Fakirov, S. Compos Sci Technol 2006, 66, 3161.
13. Hussain, F.; Hojjati, M. J Compos Mater 2006, 40, 1511.
14. Ray, S. S.; Okamoto, M. Prog Polym Sci 2003, 28, 1539.
15. Si, M.; Araki, T.; Ade, H.; Kilcoyne, A. L. D.; Fisher, R.; Sokolov, J. C.; Rafailovich, M. H. Macromolecules 2006, 39, 4793.
16. Qu, C.; Yang, H.; Liang, D.; Cao, W.; Fu, Q. J Appl Polym Sci 2007, 104, 2288.
17. Ray, S. S.; Pouliota, S.; Bousminaa, M.; Utrackib, L. A. Polymer 2004, 45, 8403.
18. Xu, X. B.; Li, Z. M.; Yang, M. B.; Jiang, S.; Huang, R. Carbon 2005, 43, 1479.
19. Dai, K.; Xu, X. B.; Li, Z. M. Polymer 2007, 48, 849.
20. Evstatiev, M.; Fakirov, S.; Evstatiev, O.; Friedrich, K. Int J Polym Mater 2004, 53, 211.
21. Evstatiev, M.; Fakirov, S. In Polymer Composites: From Nano- to Macro-Scale; Friedrich, K., Fakirov, S., Zhang, Z., Eds.; Springer: New York, 2005, Chap. 9, p 149.
22. Zhang, Q.; Yang, H.; Fu, Q. Polymer 2004, 45, 1913.
23. Wilson, J. N.; Titheridge, D. J.; Kieu, L.; Idriss, H. J Vac Sci Technol A 2000, 18, 1887.
24. Evstatiev, M.; Fakirov, S.; Krasteva, B.; Friedrich, K.; Covas, J.; Cunha, A. Polym Eng Sci 2002, 42, 826.
25. Friedrich, K.; Ueda, E.; Kamo, H.; Evstatiev, M.; Fakirov, S. J Mater Sci 2002, 37, 4299.
26. Ma, J.; Zhang, S.; Qi, Z.; Li, G.; Hu, Y. J Appl Polym Sci 2002, 83, 1978.
27. Othman, N.; Hassan, A.; Rahmat, A. R.; Wahit, M. U. Polym Polym Compos 2007, 15, 217.
28. Fornes, T. D.; Paul, D. R. Polymer 2003, 44, 3945.
29. Sui, G.; Zhong, W. H.; Fuqua, M. A.; Ulven, C. A. Macromol Chem Phys 2007, 208, 1928.
30. Bae, T. Y.; Park, K. Y.; Kim, D. H. J Appl Polym Sci 2001, 81, 1056.
31. Rong, M. Z.; Zhang, M. Q.; Pan, S. L.; Friedrich, K. J Appl Polym Sci 2004, 92, 1771.
32. Chow, W. S.; Mohd-Ishak, Z. A.; Karger-Kocsis, J.; Apostolov, A. A.; Ishiaku, U. S. Polymer 2003, 44, 7427.
33. Pothan, L. A.; Oommen, Z.; Thomas, S. Compos Sci Technol 2003, 63, 283.
34. Heino, M.; Kirjava, J.; Hietaoja, P.; La, J. S. J Appl Polym Sci 1997, 65, 241.
35. Papke, N.; Karger-Kocsis, J. Polymer 2001, 42, 1109.
36. McCrum, N. G.; Read, B. E.; Williams, G. Anelastic and Dielectric Effects in Polymeric Solids; Wiley: London, 1967.
37. Mohanty, S.; Verma, S. K.; Nayak, S. K. Compos Sci Technol 2006, 66, 538.